01 Aug 1995

# FDTD Modeling of Thin Wires for Simulating Common-Mode Radiation from Structures with Attached Cables

David M. Hockanson

James L. Drewniak
*Missouri University of Science and Technology*, drewniak@mst.edu

Todd H. Hubing
*Missouri University of Science and Technology*

Thomas Van Doren
*Missouri University of Science and Technology*, vandoren@mst.edu



## Recommended Citation

D. M. Hockanson et al., "FDTD Modeling of Thin Wires for Simulating Common-Mode Radiation from Structures with Attached Cables," *Proceedings of the IEEE International Symposium on Electromagnetic Compatibility (1995, Atlanta, GA)*, pp. 168-173, Institute of Electrical and Electronics Engineers (IEEE), Aug 1995.
The definitive version is available at https://doi.org/10.1109/ISEMC.1995.523540

# FDTD Modeling of Thin Wires for Simulating Common-Mode Radiation from Structures with Attached Cables

David M. Hockanson, James L. Drewniak, Todd H. Hubing, & Thomas P. Van Doren
Department of Electrical Engineering, Electromagnetic Compatibility Laboratory, University of Missouri–Rolla, Rolla, MO 65401

## Abstract

The analysis of shielding enclosures is complicated by the existence of apertures and cables. The Finite-Difference Time-Domain (FDTD) method can model shielding enclosures with complex geometries, but has difficulty modeling wires and cables of arbitrary radii. Modeling the wire by setting the axial component of the electric field to zero in FDTD results in a wire with a radius determined by the mesh discretization. Neglecting wire radius in applications such as Electromagnetic Interference (EMI) or printed circuit board modeling may result in gross errors because near field quantities are typically sensitive to wire thickness. Taflove developed a wire modeling algorithm for FDTD analysis which models wires well for far-field calculations such as Radar Cross Section. The method uses a quasi-static field approximation to model wires with a user-specified radius. The wire model is reviewed and investigated for near-field accuracy via input impedance computations, since FCC class A and B regulations are tested in the near field. The input impedance for a center-fed dipole antenna is computed with FDTD methods and compared to the input impedance results from moment methods. A simulation of a shielding enclosure with an attached cable demonstrates the utility of FDTD analysis in EMC applications.

## 1 Introduction

The Finite-Difference Time-Domain (FDTD) method is well documented and is not reviewed here. The reader is referred to [1], and [2] for information on FDTD.

Conducting enclosure shields are designed to minimize radiated emissions from digital electronics. However, the shielding integrity of the enclosures is compromised by apertures permitting air flow to cool internal circuits, power and peripheral cables penetrating the enclosure, seams, and display apertures. Energy can couple to the external environment as a result of these perforations in the shield. A subcellular FDTD model for wires is needed to numerically study coupling mechanisms present in complicated electromagnetic structures with external cables and predict EMI with engineering accuracy. The model must be computationally efficient and implementable. In addition to radiation through the apertures, energy coupling to an attached shielded or unshielded cable is of concern. Radiated emissions can be increased as a result of the cable, as well as the cable serving to direct energy. At the printed circuit board level, traces must be modeled well if accurate impedance results are to be computed.

Some work has been done which attempts to model wires in FDTD. Accurate results have been found by modeling with very fine discretization in the region of wires and setting the axial component of the electric field to zero [3], [4]. However, this approach does not permit modeling of wires with specific diameters, and the diamter is determined by the mesh discretization. Another method involves calculating the self-inductance of a segment of wire and developing FDTD equations for computing the necessary field quantities [5], which is not computationally efficient for large problems because of the introduction of charge and current equations. A quasi-static subcellular algorithm for modeling wires was successfully employed in FDTD for calculating far-field quantities such as Radar Cross Section (RCS) [2]. This last modeling approach is reviewed and investigated here for use in near-field calculations. A dipole antenna is modeled and the input impedance is calculated for comparison with results from the Numerical Electromagnetics Code (NEC). The quasi-static algorithm is found to have engineering accuracy in the near-field for wires less than three-quarters of a wavelength long. A shielding enclosure with an aperture and an attached shielded cable is then modeled. The power radiated through the aperture is computed with and without the attached cable and some conclusions are drawn concerning the coupling mechanisms present in the simulated enclosure.

## 2 Review of Thin Wire Model Development

Proper consideration must be given to wire modeling to enable accurate computation of near-field parameters. Wires are placed along the electric field grid because the tangential component of the electric field on the surface of a perfect electric conductor (pec) is zero. Modeling the wire by setting the axial component of the electric field to zero was found from numerical simulations to yield effective wire radii of approximately twenty percent of a cell length for cubic cells [1]. The algorithm "sets" the radius because FDTD averages the field values over a finite volume. An alternative to setting $\vec{E}_{tan} = 0$ along $\vec{E}$-field grid line and having the wire radius determined by the mesh dimensions is to employ a quasi-static approximation

[1] see Section 3

0-7803-2573-7/95/0000-0031 $4.00 © 1995 IEEE

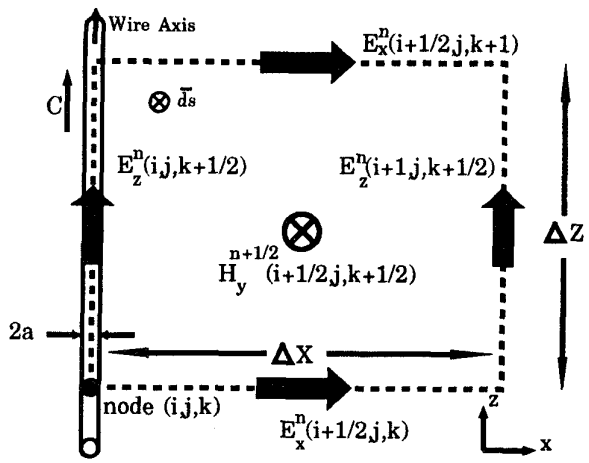


Figure 1: An example of the discrete field locations in the plane of a thin wire.

introduced for FDTD by Taflove et al. [2]. This approach is summarized briefly herein.

Figure 1 shows a pec wire of radius $a$ superimposed on a Yee mesh, and discrete FDTD field locations in the plane of the wire. For sufficiently small cells, the electric field component parallel to the wire $E_z(i+1)$, can be approximated as a linear function in $z$. A quasi-static approximation $(\frac{1}{r})$ is employed for the functional variation of the fields in the transverse direction radial to the wire axis. Ampere's law in integral form can then be evaluated using the quasi-static approximations, where the integration paths are shown in Figure 1. Discretizing the result of Ampere's law and rearranging yields the update equation for the magnetic field components adjacent to the wire. For example, $H_y(i+\frac{1}{2}, j, k+\frac{1}{2})$ near a thin wire of radius $a$ oriented in the $\hat{z}$ direction is given by

$$\begin{aligned} H_y^{n+\frac{1}{2}}(i+\frac{1}{2},j,k+\frac{1}{2}) = \quad & H_y^{n-\frac{1}{2}}(i+\tfrac{1}{2},j,k+\tfrac{1}{2}) \\ & -\tfrac{\Delta t}{\mu}\left[\left(E_z^n(i+\tfrac{1}{2},j,k+1)\right.\right. \\ & \left.\left.-E_z^n(i+\tfrac{1}{2},j,k)\right)\tfrac{1}{\Delta x}\right. \\ & \left.-\frac{E_z^n(i+1,j,k+\frac{1}{2})}{\frac{\Delta x}{2}\ln\frac{\Delta x}{a}}\right]. \end{aligned} \quad (1)$$

The other three magnetic field components surrounding the wire are found similarly. The tangential component of to the electric field components is $\vec{E}$ is set to zero along the wire axis. Similar equations can be developed for the magnetic fields circulating thin wires with orientations in the $\hat{x}$ and $\hat{y}$ directions.

# 3 Thin Wire Model Evaluation

The algorithm outlined in the previous section was originally developed by Taflove et al. for far-field RCS computations. Because of its computational efficiency and simplicity, this algorithm was investigated for near-field computations with engineering accuracy useful for EMC analyses such as determining EMI and modeling coupling mechanisms at the printed circuit board level. The accuracy of this thin-wire algorithm for near-field calculations

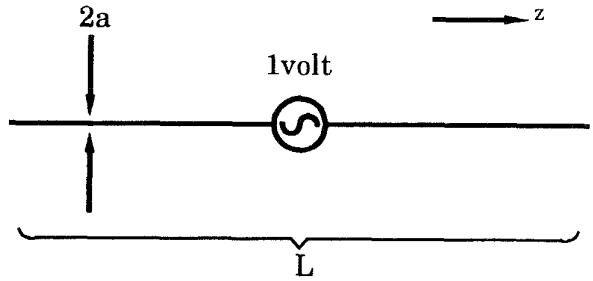


Figure 2: Geometry of the dipole antenna model.

was evaluated by modeling a dipole antenna. The input impedance was calculated for a center-fed dipole over a range of frequencies. The antenna was modeled using the FDTD method and compared to moment method results obtained with the Numerical Electromagnetics Code (NEC).

Figure 2 shows the dipole antenna that was modeled numerically by NEC and the FDTD method. A voltage source for the FDTD model was implemented by setting $E_z$ to a specified value. The field value was determined by the static discrete voltage equation $E = -\frac{V}{\Delta l}$. The FDTD model of the source differed from that employed by the moment method in that the FDTD source had a finite length (the length of a cell side), and the moment method modeled a point source (delta-gap generator). The radius of the wire $a$, was varied to determine the accuracy of the FDTD quasi-static near-field approximation for a *thin* wire (less than the unit cell dimensions). The impedance was calculated for the dipole antenna as a function of the ratio of length $L$, to wavelength $\lambda$, over the range $0.25 \leq \frac{L}{\lambda} \leq 1$. Other dimensions are given in terms of the ideal half-wave resonance wavelength, which is denoted by $\lambda_o \equiv 2L$.

The dipole antenna was first modeled by setting the tangential electric field component on the wire axis to zero, and computing the surrounding magnetic field components with the usual free-space FDTD equations. Cubic cells were employed with a spatial discretization of $\Delta l = \frac{\lambda_o}{42}$, and a differential time element of $\Delta t \approx \frac{\Delta l}{2c_o}$ [2], where $c_o$ is the free-space phase velocity. A time-harmonic source was employed and each impedance value was computed after the system had reached steady-state. The antenna length was held constant at each simulation frequency, and was twenty-one cells long. Perfectly Matched Layer (PML) boundary conditions were employed six cells from the antenna and were four cells thick providing a reflection coefficient of -60dB [6]. The input impedance results computed with the FDTD method are compared with NEC results in Figure 3. Several NEC simulations using different wire radii were run to find a best fit to the FDTD results. As seen in Figure 3, with the tangential electric field along the wire axis set to zero, seemingly approximating an infinitely thin wire, the FDTD computations result in a wire of finite thickness. The reason

[2]The time-step is approximate because it was minutely changed for each frequency in order to allow an integer number of time-steps per cycle

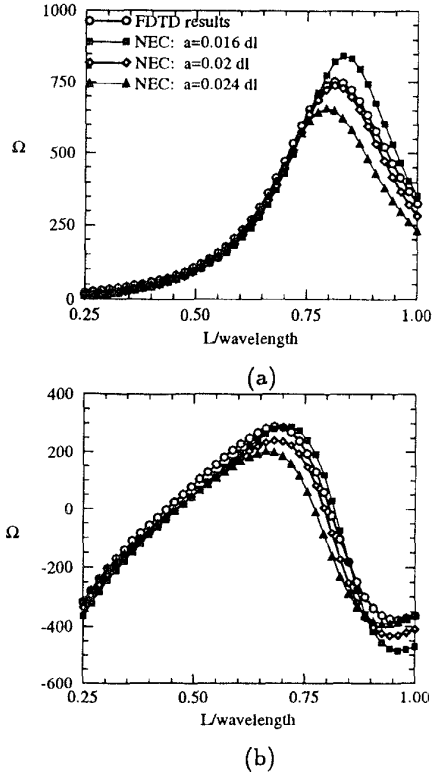


Figure 3: The FDTD input impedance results for an antenna modeled without defining a radius for a) input resistance, and b) input reactance ($dl \equiv$ FDTD cell length).

is because the FDTD method computes the *average* of the field component over a finite volume and assigns it to the location associated with the unit cell. The averaging process results in an effective wire radius dictated by the mesh dimensions. Figure 3 shows that the FDTD results agree best with the NEC results for a wire of radius $a = 0.005\lambda_o$. The effective radius of a wire modeled with the FDTD method by setting $\vec{E}_{tan} = 0$ along a grid axis is then approximately twenty percent of the cell dimension. The half-wave resonance frequency computed by the FDTD code differed by less than three percent from that computed by NEC for an antenna with a radius $a = 0.005\lambda_o$ (approximately twenty percent of the FDTD cell dimension). However the resistance at the half-wave resonance differed by approximately 8.5%.

Taflove's quasi-static approach was also employed for modeling thin wires with the FDTD method. The wire radius could then be well defined. Figure 4 shows a comparison of input impedance results for a center-fed dipole from the FDTD code, and NEC, when the FDTD model included conductors with a set radius. The magnetic field components circulating the source were calculated with free-space FDTD update equations. The magnetic field components surrounding the wire were computed with Taflove's quasi-static approximations. The results show poor agreement between the two methods, in particu-

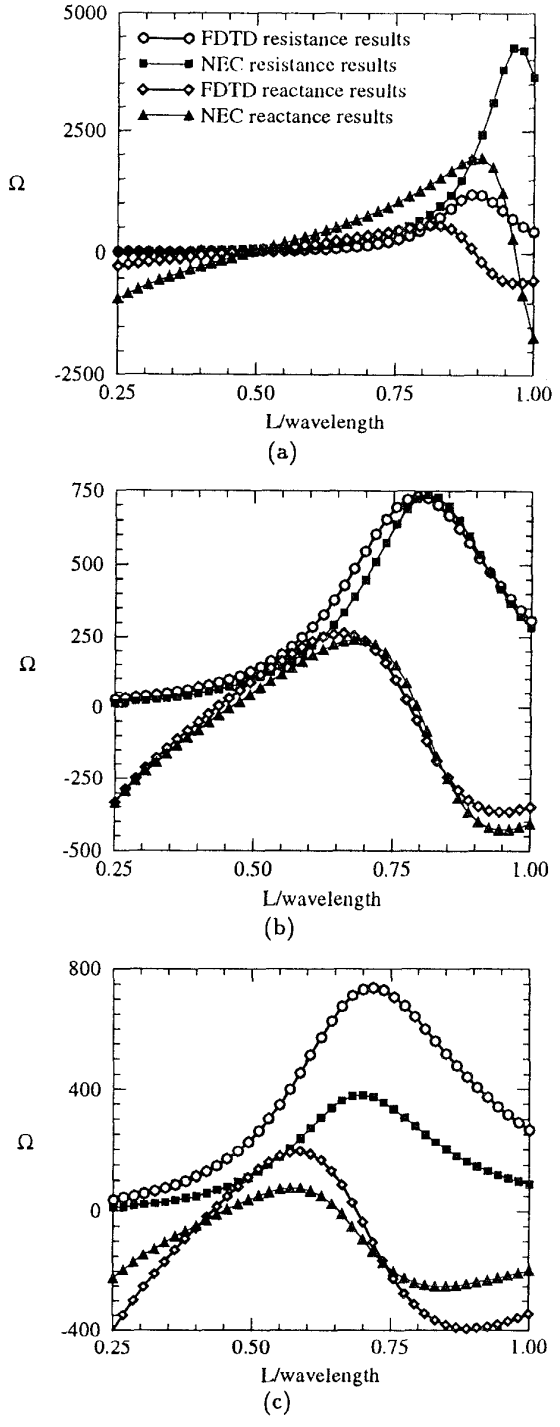


Figure 4: Input impedance comparison between FDTD results and NEC results for a dipole antenna with a set conductor radius, but no defined source radius for a) *very thin*, $a = 0.002\Delta l = \frac{\lambda_o}{21{,}000}$, b) *thin*, $a = 0.2\Delta l = \frac{\lambda_o}{210}$, and c) *thick*, $a = 0.48\Delta l = \frac{\lambda_o}{87.5}$ wires.

lar the input resistance. The discrepencies resulted from an inaccurate source model. The source model experienced an effective radius dictated by the mesh dimensions because the magnetic field components adjacent to the source were not modified. Figure 4b shows reasonable agreement because the wire radius was the same as the effective radius of the source.

For a more accurate model, the source was given the same radius as the conductors using Taflove's quasi-static approximations. The input impedance for a center-fed dipole was computed for wires of three different radii. The FDTD results are compared with NEC results in Figure 5. The *thin* wire ($a = 0.2\Delta l$) results in Figure 5b agreed well with the NEC results for dipole lengths less than $\frac{3}{4}\lambda$. In many cases of EMI, the antennas are less than $\frac{3}{4}\lambda$. In addition, many of the modeling details at the printed circuit board level are small in terms of wavelength. The FDTD computed half-wavelength resonance frequency was within three percent of that computed by NEC, and the input resistance at resonance was within one percent. This is expected, since the antenna radius is set very close to the effective radius of $0.2\Delta l$ established by the FDTD algorithm. The *very thin* and *thick* wires showed good agreement with the NEC computations up to $L = \frac{3}{4}\lambda$ as well. The half-wavelength resonance frequency computed with FDTD was within five percent for both the *very thin* and *thick* wires, and the resistance at resonance was within three percent. At higher frequencies (shorter wavelengths) the source length becomes appreciable in terms of the wavelength if the spatial discretization is left unchanged. The electrically long source may account for the discrepencies between the two methods for $L > \frac{3}{4}\lambda_o$, since the moment method employs a delta-gap generator.

The quasi-static approximation limits the wire radius to $a < \frac{\Delta l}{2}$, because the magnetic field calculation is unstable when the wire radius approaches the location of the tangential magnetic field components. The field dependence does not have the same $r$ variation if the fields are located inside the wire. The approximation could be reformulated for the case of wires with radii greater than $\frac{\Delta l}{2}$, however such a wire may be more easily modeled by placing the wire inside a cell and setting the tangential electric field components to zero.

# 4 Shielding Enclosure Model

A rectangular shielding enclosure with a narrow aperture was modeled to study radiation from conducting enclosures with attached cables. All dimensions reported herein were normalized to the free-space wavelength at the lowest predicted ideal (continuous rectangular cavity) $TE_{101}$ cavity resonance, $\lambda_o \equiv 2\frac{1}{\sqrt{\frac{1}{width^2}+\frac{1}{depth^2}}}$. The computational domain was discretized with cubic cells of dimension $\Delta l = \frac{\lambda_o}{20} = \Delta x = \Delta y = \Delta z$. The differential time element was $\Delta t \approx \frac{\Delta l}{2c_o}$, where $c_o$ was the speed of light in free-space. The cavity model, shown in Figure 6, had dimensions of $1.2\lambda_o \times .25\lambda_o \times .55\lambda_o$. The enclosure walls were modeled as pec's. The aperture was $.3\lambda_o \times .05\lambda_o$, and

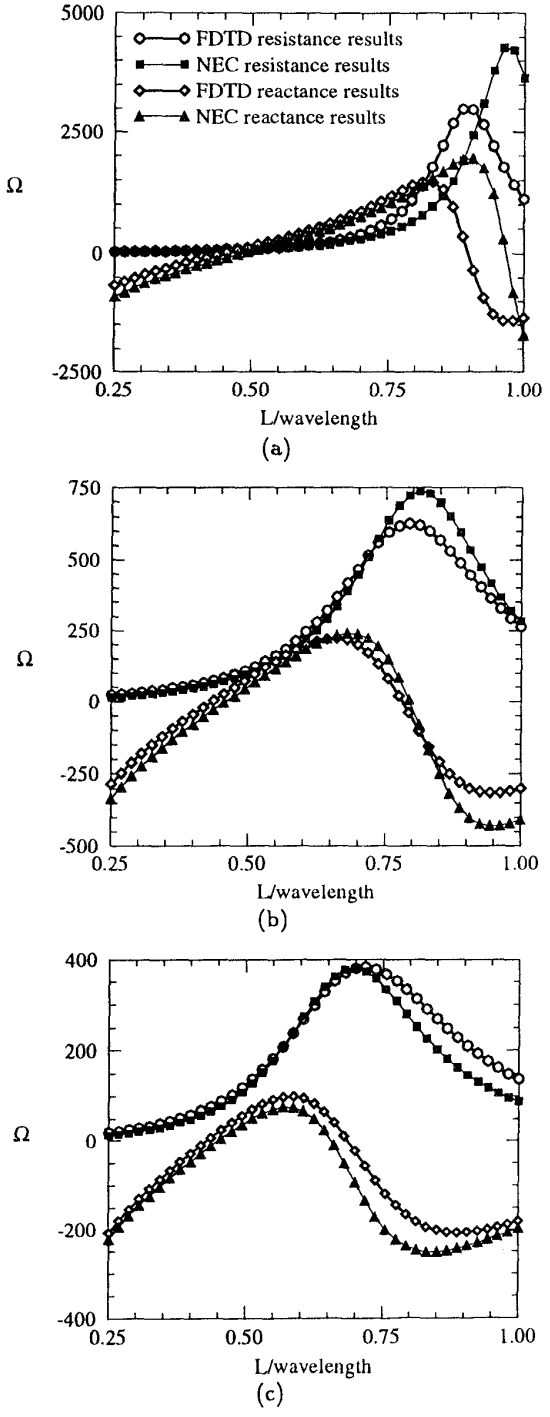


Figure 5: Input impedance comparison between FDTD results and NEC results for a dipole antenna with set source and conductor radii for a) *very thin*, $a = 0.002\Delta l = \frac{\lambda_o}{21{,}000}$, b) *thin*, $a = 0.2\Delta l = \frac{\lambda_o}{210}$, c) *thick*, $a = 0.48\Delta l = \frac{\lambda_o}{87.5}$ wires.

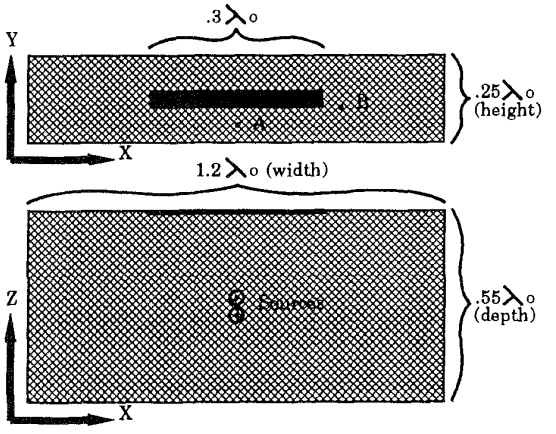


Figure 6: Longitudinal and transverse planar views of the shielding enclosure showing the dimensions and location of the attached cables and the aperture.

centered in the pec wall. The cavity was excited with two $1\frac{A}{cm^2}$ $\hat{y}$-polarized, in-phase, current density sources. Two sources were used to provide symmetry inside the cavity. The sources were located in the center of the enclosure. Second order Mur absorbing boundaries were located one-half free-space wavelength from the enclosure. The sources were swept in frequency between $.8 \leq \frac{f}{\frac{c_o}{\lambda_o}} \leq 1.8$. The time-averaged power through the aperture was computed at each frequency. All radiated powers were normalized to the radiated power level computed for the lowest cavity resonance ($TE_{101}$) for the base (control) configuration of a cavity with an aperture (i.e. no attached cables).

The sources of the control configuration were swept in frequency and the power radiated through the aperture was determined. The power-frequency response for the control configuration is shown in Figure 7. Approximately twenty-five points were computed around the peaks to ensure that a peak value had been computed. The lower resonance was the lowest cavity resonance, hereafter referenced as the $TE_{101}$ mode . This resonance was shifted down in frequency from the theoretical value for a continuous rectangular cavity because of the aperture. The aperture dimensions at the $TE_{101}$ resonance were small relative to wavelength, resulting in very little loss to the system and a $Q$ of over 500. For typical applications, an enclosure would have numerous apertures and seams, and $Q$'s less than 100 might be expected. The $Q$ is defined here as the ratio of radian frequency times the stored energy to dissipated power, which is equivalent to $\frac{f_{peak}}{\Delta f_{3dB}}$ where $f_{peak}$ is the resonance frequency, and $\Delta f_{3dB}$ is the difference between the 3dB frequencies.

The second cavity resonance, the $TE_{201}$ mode, should have occured at a normalized frequency of 1.233. Since the field distribution was even about the source in $x$, and the sources were in phase, only modes with even symmetry about the source in $x$ were excited. Because of the source locations, the source was orthogonal to the $TE_{201}$ mode and did not excite it. Even modes, such as the $TE_{201}$ mode, required a null at the center of the cavity where the sources were located. The resulting low energy emission demonstrated how source location could affect EMI.

The last cavity resonance within the observed frequency range ($TE_{301}$), expected at $f_{normalized} \approx 1.54$, was shifted down because of the loss through the aperture. The aperture had a half-wave resonance at $f_{normalized} \approx 1.67$ which was shifted down due to the finite width of the aperture. The proximity of the aperture resonance and $TE_{301}$ mode resonance created a broadband region in the power-frequency response.

A wire was attached to the shield face containing the aperture to investigate coupling through the aperture to the wire. The time-averaged power through the aperture as a function of frequency is shown in Figure 7 for a wire attached at location $A$, and then at location $B$ [3]. A shielded wire was modeled with Taflove's quasi-static field approximation as described in Section 2. The wire connection to the shield was modeled by using quasi-static approximations to compute the magnetic field components surrounding the wire, and setting the electric field components along the wire axis, and tangential to the shield to zero. This configuration was employed to model a shielded cable attached to the enclosure at all 360° around the cable. The wire had a length of $\frac{\lambda_o}{5}$ ($= 4\Delta l$) and a radius of $\frac{\lambda_o}{250}$ ($= .08\Delta l$). The wire was located alternately at points $A$ and $B$ in Figure 6, where point $A$ was horizontally centered and $\frac{\lambda_o}{20}$ below the edge of the aperture, and $B$ was $\frac{\lambda_o}{20}$ to the right of the lower right hand corner of the aperture. The wire should have resonated at $f_{normalized} \approx 1.25$. As previously discussed, the field distribution in the cavity at this frequency was odd in $x$ , however, the source distribution was even thereby not exciting this mode.

An attached shielded cable reduced the power radiated through the aperture at the $TE_{101}$ resonance. Equivalence theory can be employed to replace the electric field over the aperture in a pec plane with magnetic current sources for discussion purposes. At lower frequencies the aperture was short with respect to wavelength and the magnetic currents looked like a short magnetic dipole. The wire attached at $A$ was located where the $\hat{z}$-component of the electric field was at a maximum in the magnetic dipole radiation pattern. Energy coupled efficiently to the wire at $A$ providing an effective loss mechanism. The $Q$ at the $TE_{101}$ resonance was consequently reduced. The wire at $B$ was located where the $\hat{z}$-component of the electric field was at a low level in the dipole radiation pattern; therefore the $Q$ was not reduced to the same degree as with the wire located at $A$.

At the $TE_{301}$ mode resonance frequency, the addition of the wires "tuned" the system resulting in an increased $Q$. The peak radiated power was increased by approximately 3 dB. In addition, the wire can potentially increase the directivity of the radiated energy. The FCC guidelines limit maximum field strength, and therefore, the addition of shielded cables to the system may make the device fail emissions testing. Further study is necessary to understand the mutual coupling between the aperture and shielded cables, as well as potential directivity of energy

[3] see Figure 6

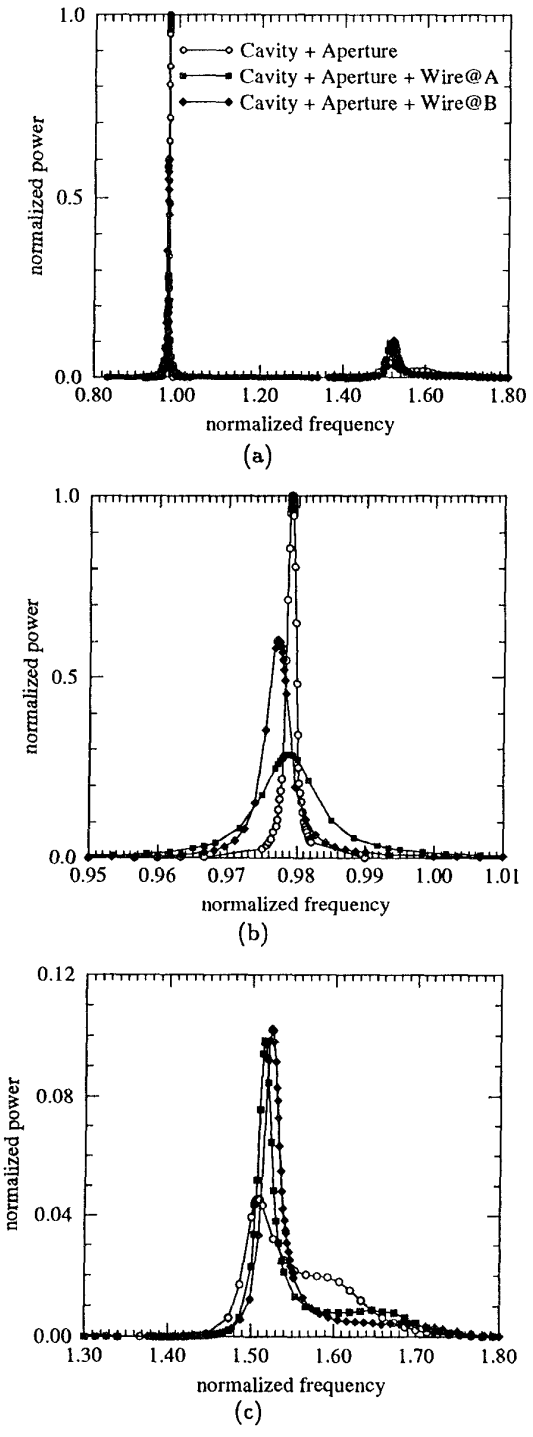


Figure 7: The time-averaged power through the aperture as a function of frequency for the shielding enclosure with an aperture, the shielding enclosure with an aperture and a wire attached at $A$, and the shielding enclosure with an aperture and a wire attached at $B$. a) Entire frequency range, b) enlarged view of lower resonance, and c) enlarged view of upper resonance.

by the wire.

# 5 Conclusion

The discrepencies found in the verification of the wire modeling algorithm occurred mainly because of different source models used in the two computational methods (FDTD and moment method). The quasi-static field approximation for wire modeling developed by Taflove was found to be acceptable for many EMC applications for wires on the order of a wavelength long. For example, the model should be sufficient for modeling shielded or unshielded cables penetrating a shielding enclosure where the cable is typically small at the frequencies of interest, or modeling many aspects of printed circuit boards. The advantage to this approach when compared to other alternatives is the ease of development and the small increase in required computational resources.

The quasi-static algorithm was used to model a cable attached to a shielding enclosure with an aperture. The results were provided to demonstrate the utility of the algorithm, although a comparison between experimental or other numerical results was not yet available.

# References

[1] K. S. Kunz and R. J. Luebbers, *The Finite Difference Time Domain Method for Electromagnetics*, CRC Press, Boca Raton, Florida, 1993.

[2] A. Taflove and K. Umashankar, "The finite-difference time-domain method for numerical modeling of electromagnetic wave interactions", *Electromagnetics*, vol. 10, pp. 105–126, 1990.

[3] J. G. Maloney, G. S. Smith, and Jr. W. R. Scott, "Accurate computation of the radiation from simple antennas using the finite-difference time-domain method", *IEEE Transactions on Antennas and Propagation*, vol. 38, pp. 1059–1068, July 1990.

[4] R. J. Luebbers, L. Chen, T. Uno, and S. Adachi, "Fdtd calculation of radiation patterns, impedance, and gain for a monopole antenna on a conducting box", *IEEE Transactions on Antennas and Propagation*, vol. 40, pp. 1577–1583, December 1992.

[5] R. Holland and L. Simpson, "Finite-difference analysis of emp coupling to thin struts and wires", *IEEE Transactions on Electromagnetic Compatibility*, vol. 23, pp. 88–97, May 1981.

[6] J. P. Berenger, "A perfectly matched layer for the absorption of electromagnetic waves", *Journal of Computational Physics*, accepted for publication 1994.